Measurements of Density Scale Length Dependence of Brillouin Backscatter from Laser Produced Plasmas

R. E. Turner

Report No. 105
June, 1980

I. INTRODUCTION

Controlled thermonuclear fusion holds forth the promise of a virtually inexhaustable energy supply for mankind, and has, therefore, received considerable attention from researchers over the past three decades. Since the fuel, isotopes of hydrogen, must be heated to temperatures of over 1 KeV, it is fully ionized, and rich in the phenomena of plasma physics. While most of the research effort has focused on magnetic confinement, another approach, laser driven inertial confinement, became possible with the advent of high power laser systems. The basis of this approach is to use a laser to compress and heat a fuel pellet to high enough densities and temperatures that a significant number of thermonuclear reactions take place before the pellet disassembles. The basic ideas have been reviewed by a number of authors[1,2].

One of the plasma physics problems of obvious importance is the absorption of the laser light by the plasma. Ideally, one would hope to have all of the light absorbed and used to heat and compress the fuel. The 'classical' absorption of light by a plasma is due to electron-ion collisions, which randomize the electrons' otherwise ordered motion in the electromagnetic field[2].

Since the collision rate is proportional to the density squared[2], collisional absorption is ineffective at low densities. To give a specific example, consider light of one micrometer wavelength incident on a plasma which has an electron temperature of one kilovolt. Collisional absorption is significant only if the density profile is slowly varying (e.g., $L > 30$ μm, where L is the density scale length, n is the electron density, and $L = n(dn/dx)^{-1}$), and then only near the critical surface. The critical surface is the region where the local plasma frequency ($\omega_p^2 = 4\pi ne^2/m$) equals the laser frequency, and beyond which light cannot propagate.

Resonant absorption[3] is thought to be the principle absorption mechanism in current short pulse, small density scale length experiments. The laser light can stimulate the growth of plasma waves at the critical surface; the energy in the plasma waves is then coupled to the electrons either through Landau damping[4], or, in the case of high intensities, wave breaking[5], which generates high energy electrons. The plasma waves are strongly driven only at the critical surface, where their frequency is resonant with that of the incoming laser light.

There are still other candidates for explaining 'anomalous' absorption, such as the parametric decay instability[6]. However, all the absorption mechanisms share a common characteristic; they require the laser

light to propagate to the vicinity of the critical surface. Any plasma instability which hinders this will therefore reduce the absorbed energy, making compression and heating more difficult. One such instability is stimulated Brillouin scattering[6-9].

Brillouin scattering is a three wave parametric instability involving an incident electromagnetic wave, an ion-acoustic wave, and a scattered electromagnetic wave. The scattered wave is very nearly at the same frequency as the incident wave, differing only by the ion-acoustic frequency, which is typically three orders of magnitude smaller than the electromagnetic frequencies. Therefore, the energy in each scattered photon (Planck's constant times the frequency) is very nearly equal to the incident photon's energy; Brillouin scattering can reflect a large fraction of the incident light. As will be shown in chapter II,the instability depends on the ion-acoustic wave being resonantly driven by the beat between the incident and scattered electromagnetic waves. This resonance, or matching condition, can, in general, be satisfied only locally in a plasma with density and velocity gradients. As the gradients become smaller, the conditions for growth of the instability become more favorable. Furthermore, the saturation of the instability, thought to be due to ion heating[10] or ion trapping[11],

will occur at a higher level for a more homogeneous plasma, due to the larger number of ions within the scattering region.

Brillouin scattering is a cause of some concern when one considers the pulse shapes planned for future fusion experiments. Most previous experiments used relatively short, fast rising pulses of 30 to 200 nsec, illuminating thin shells, which resulted in 'exploding pusher' behavior; the shell of the target is rapidly heated and explodes, resulting in multi-kilovolt core temperatures, and densities of 0.2 gm/cm^3 (liquid D-T) or less. There is relatively little underdense plasma present during the laser pulse. In addition, the high intensities cause density profile steepening around the critical surface, further suppressing parametric instabilities. High core densities are not reached, however. Therefore, alternative pulse shapes are now under consideration, or being used, to provide 'ablative pusher' type implosions. Long pulses, 1 nsec or more, starting at low intensities and slowly rising to high intensities, are to be used to ablate away the outside of the target without shock-heating the fuel. As the plasma streams away, the reaction forces will drive the remaining shell inward, compressing the fuel. However, the large amount of underdense plasma produced may be

ideal for the growth of Brillouin scattering, which could reflect the laser light before it has reached the critical surface, and thus reduce the amount of energy absorbed. Thus it is important to be able to predict the amount of Brillouin scattering present in such a situation. Various models and computer simulations have attempted to do this. Their predictions depend on a number of parameters, including laser wavelength and intensity, electron and ion temperatures, and velocity and density profiles. The main thrust of this thesis has been to measure the effect of various density profiles on stimulated Brillouin scattering. In addition, insight into the behavior of this instability in the high intensity, non-linear regime, is provided by temporally resolved backscatter spectral data. To simulate the effects of a shaped pulse, we have used a short (60 psec FWHM), high intensity pulse to irradiate a pre-pulse generated plasma.

Others have examined the behavior of stimulated backscatter, but with different diagnostics, geometry, and/or laser parameters, than the work presented here. Ripin[12], et al., measured backscatter off of plane targets, using a prepulse to create a (presumed) plane plasma. A Raman shifted probe beam measured the density profile. However, the relatively long wavelength of the

probe (6329 Å) restricts the measurement to densities of approximately 10^{19} cm^{-3} or less, far removed from the critical surface. Additionally, the plane geometry can result in a steady state velocity flow profile considerably different from that which occurs with spherical targets. Phillion, et al.[10], measured Brillouin scattering from plane targets irradiated with moderately long pulse widths (150 to 400 psec) and large (100 to 250 μm) focal spots. The density scale lengths were not measured; they were estimated as being comparable to the focal spot radius. The laser pulse was not preceded by a prepulse. The backscatter spectra were dominated by the large outward expansion velocity of the plasma, and consequently show a Doppler shift toward shorter wavelengths. The authors also present a model, based on strong ion heating and consequent large Landau damping, to estimate the total amount of backscattered energy. This model will be reviewed in chapter II, and compared with our data in chapter VI.

We have attempted, in this thesis, to simulate laser fusion experiments with shaped pulses, and to measure the density profiles in the region of greatest importance, e.g., near critical density. To this end, we have used prepulses to create sizeable underdense plasmas, similar to the effect of long, low intensity

pulses; and, we have used an ultraviolet probe beam, capable of measuring electron densities up to 10^{21} cm^{-3}, to measure the density profiles. Density scale lengths obtained ranged from 5 to 50 micrometers.

Our results support the ion-heating theory of Kruer[10], in that a relatively slow increase in back-scattered energy is observed with increasing density scale lengths. The time integrated backscatter spectra show the red shift characteristic of Brillouin scattering.

The time resolved spectra reveal an interesting mode structure in the backscattered light. Several possible explanations of this data will be discussed in chapter VI. This data should be useful in pointing the way toward an increased theoretical understanding of Brillouin scattering.

II. THEORY OF STIMULATED BRILLOUIN BACKSCATTER

A. Linear Theory For Homogeneous Plasmas

In this section, the linearized theory of Brillouin scattering is reviewed. This theory has been covered extensively in the published literature[1,2,3,4]; we will mainly follow the treatment given by Forslund, et al.[4] The basic fluid and Maxwell equations are:

$$\frac{\partial}{\partial t}\underline{v}_\alpha + \underline{v}_\alpha\cdot\nabla\underline{v}_\alpha = \frac{q_\alpha}{M_\alpha}\left[-\nabla\phi - \frac{1}{c}\frac{\partial}{\partial t}\underline{A} + \frac{1}{c}\,\underline{v}_\alpha\times(\nabla\times\underline{A})\right] + -\gamma_\alpha T_\alpha \nabla N_\alpha/(M_\alpha N_\alpha) \tag{1}$$

$$\frac{\partial}{\partial t}N_\alpha + \nabla\cdot(N_\alpha\underline{v}_\alpha) = 0 \tag{2}$$

$$\nabla^2\underline{A} - \frac{1}{c^2}\frac{\partial^2}{\partial t^2}\underline{A} = -\frac{4\pi}{c}\underline{J} + \frac{1}{c}\frac{\partial}{\partial t}\nabla\phi \tag{3}$$

$$\nabla^2\phi = -4\pi\sum_\alpha q_\alpha N_\alpha \tag{4}$$

where α denotes the species (ion or electron), N the number density, $\underline{v}$ the fluid velocity, T the temperature, q the charge, M the mass, and $\underline{J}$ the current. γ is the ratio of specific heats (c_p/c_v), and $\underline{A}$ and ϕ are the usual vector and scalar potentials. Implicit in equation (3) is the choice of the Coulomb gauge ($\nabla\cdot\underline{A} = 0$). We will consider only waves in the $\underline{\hat{x}}$ direction; i.e.,

$$\nabla \equiv \underline{\hat{x}}\cdot\frac{\partial}{\partial x} \quad . \tag{5}$$

Linearizing equation (1), and looking only at motions in the y-z plane, we see that

$$\underline{v}_\alpha = -(q_\alpha/M_\alpha c)\underline{A} \tag{6}$$

to lowest order. Now breaking the density into a homogeneous term plus a spatially dependent pertubation, we have

$$N_\alpha = N_{o\alpha} + n_\alpha(x) \tag{7}$$

The current is then given by

$$\underline{J} = -e\underline{v}_e(N_o + n_e) \tag{8}$$

where we have neglected the contribution due to the ion motion. Using equations (5) and (8), the electromagnetic wave equation (3) becomes

$$-\left\{\frac{\partial^2}{\partial t^2} + \omega_D^2 - c^2\nabla^2\right\}\underline{A} = \omega_p^2\,\frac{n}{N_o}\underline{A} \tag{9}$$

Lack of a species subscript should be understood to refer to electrons; i.e., N_o is the homogeneous, unperturbed part of the electron number density.

To develop an equation for the density perturbation, we take the divergence of equation (1), neglect v_x in the non-linear convective terms, substitute for $\underline{v}$ with equation (2), using

$$\nabla\cdot(N_\alpha\underline{v}) = N_{o\alpha}\nabla\cdot\underline{v} \tag{10}$$

and we have

$$\frac{\partial^2}{\partial t^2}\,n = \frac{-e}{m}\,N_o\nabla^2\phi + (e/mc)^2(N_o/2)\,\nabla^2(\underline{A}\cdot\underline{A}) +$$

$$+ (\gamma\,T_e/m)\,\nabla^2 n \tag{11}$$

for the electrons, and

$$\frac{\partial^2}{\partial t^2} n_1 = (e N_o/M_1) \nabla^2\phi + (\gamma_1 T_1/M_1) \nabla^2 n_1 \qquad (12)$$

for the ions. In the ion equation, we have used $ZN_{o1} = N_o$, and the motion due to the electromagnetic field has been neglected. Now, for Brillouin scattering, we are interested in slow moving (acoustic) waves, so that the quasi-neutral approximation may be applied to the perturbed quantities everywhere except in Poisson's equation. That is, $n = n_e = Zn_1$ but $\nabla^2\phi \neq 0$. Eliminating $\nabla^2\phi$ between equations (11) and (12), and using $(Zm/M_1)<<1$, gives

$$\left[\frac{\partial^2}{\partial t^2} - c_s^2\nabla^2\right] n = N_o \frac{Ze^2}{2mMc^2} \nabla^2(\underline{A}\cdot\underline{A}) \qquad (13)$$

where

$$c_s^2 = (ZT_e + 3T_1)/M_1 \qquad (14)$$

In equation (14), the ratios of specific heats have been chosen appropriately for an acoustic wave; $\gamma_e = 1$ (isothermal), $\gamma_1 = 3$ (adiabatic).

Equations (9) and (13) form a pair of coupled equations describing the parametric interaction of the electromagnetic waves and an ion-acoustic wave. The normal modes of these waves are on the left hand side of the equations; the driving terms are on the right hand side. It should be clear that if a driving term

contains a component at the normal mode (resonance) frequency of one of the waves, that wave will experience exponential growth.

We now consider the particular case of circular polarization. Let

$$\underline{A}_o(x,t) = A_o\left[-\hat{\underline{y}}\cos(\omega_o t - k_o x) + \hat{\underline{z}}\sin(\omega_o t - k_o x)\right] \tag{15}$$

where $\omega_o^2 = \omega_p^2 + k_o^2 c^2$.

It is assumed that equation (15) satisfies the left hand side of equation (9). Let the backscattered wave be given by

$$\underline{A}_1(x,t) = A_{1y}\,\hat{\underline{y}}\cos(\omega_1 t - k_1 x) + A_{1z}\,\hat{\underline{z}}\sin(\omega_1 t - k_1 x) \tag{16}$$

and the ion-acoustic wave by

$$n(x,t) = n\cos(\omega_2 t - k_2 x) \tag{17}$$

We will use exponential notation for convenience. Substituting the expressions (16) and (17) into equations (9) and (13), and using care to keep the right hand side real, we have

$$(-\omega_1^2 + \omega_p^2 + k_1^2 c^2)\left(A_{1y}\, e^{i\omega_1 t - ik_1 x} + C.C.\right) = -(\omega_p^2/N_o)(1/2)\left(n\, e^{i\omega_2 t - ik_2 x} + C.C.\right)\left(-A_o e^{i\omega_o t - ik_o x} + C.C.\right) \tag{18}$$

and

$$(-\omega_2^2 + c_s^2 k_2^2)(n\, e^{i\omega_2 t - ik_2 x} + C.C.) =$$

$$\frac{Ze^2 N_o}{2mMc^2}\nabla^2\left[(-A_o e^{i\omega_o t - ik_o x} + C.C.)(A_{1y} e^{i\omega_1 t - ik_1 x} + CC) + \right.$$

$$\left.(-i)(A_o e^{i\omega_o t - ik_o x} + CC)(A_{1z} e^{i\omega_1 t - ik_1 x} + CC)\right] \tag{19}$$

where C.C. stands for complex conjugate of the preceding term. In equation (19) the terms $\underline{A}_o \cdot \underline{A}_o$ and $\underline{A}_1 \cdot \underline{A}_1$ have been dropped, since they have no components at the low frequency ω_2, and are therefore unimportant in driving the instability. The equation for A_{1z} is identical to equation (18) with the replacement

$$A_{1y} = -A_{1z} \quad . \tag{20}$$

Since we will see shortly that k_1 is negative (i.e., $\underline{A}_1$ is backscattered), equation (20) shows that for a left circularly polarized incident wave, the backscattered wave is right circularly polarized, and vice versa.

Knowing that the acoustic frequency ω_2 is much less than the electromagnetic frequencies ω_o and ω_1, we see that equations (18) and (19) can be satisfied only if

$$\omega_o = \omega_1 + \omega_2^* \tag{21}$$

and $$k_o = k_1 + k_2^* \tag{22}$$

These are called the matching conditions. One sees the quantum mechanical analog by multiplying these equations by $(h/2\pi)$; equations (21) and (22) then represent conservation of energy and momentum, respectively. We also see that, as illustrated in Figure 1, $k_2 = 2k_o = -2k_1$.

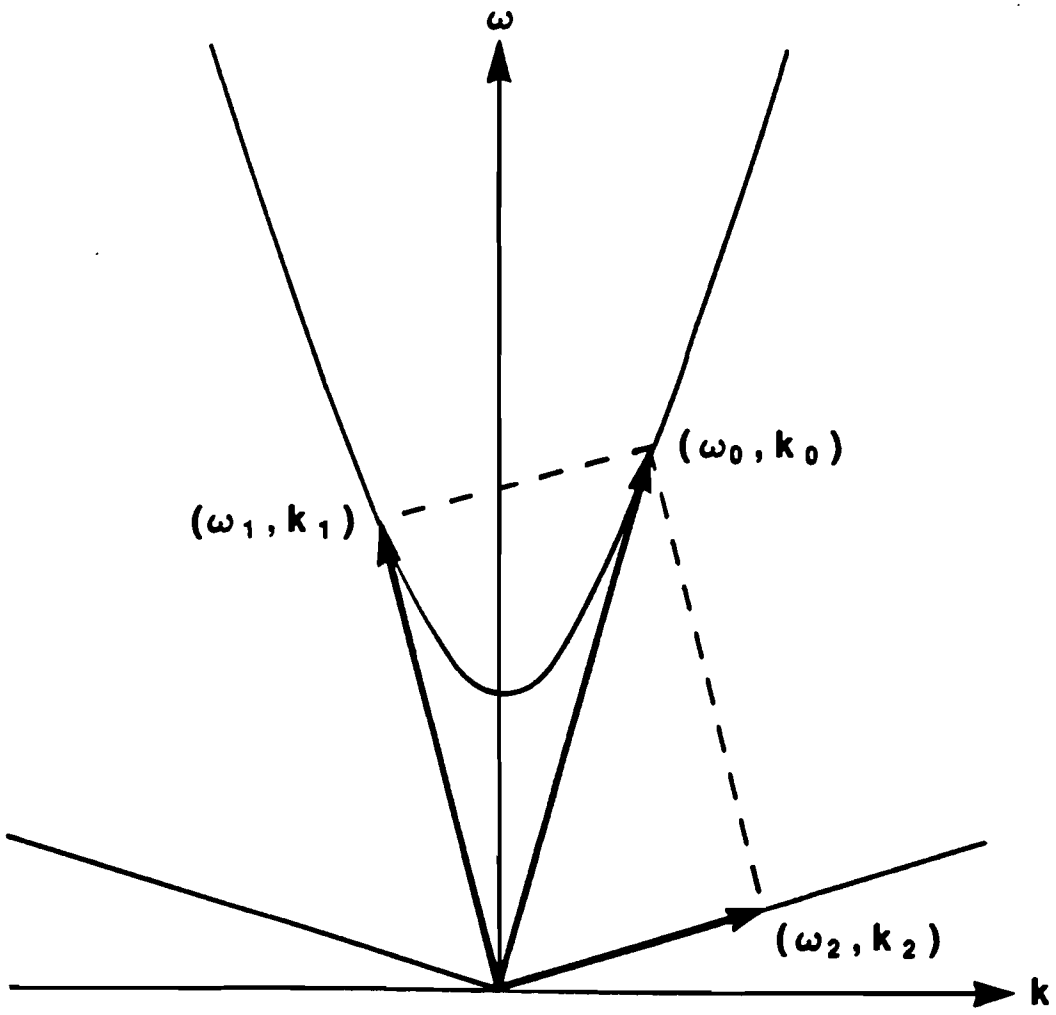

Figure 1. An (ω,k) diagram. The upper curve is the dispersion relation for an electromagnetic wave; the lower, for an ion-acoustic wave (shown with a greatly exaggerated slope, for clarity). The vector-like construction guarantees that the matching conditions will be satisfied.

Keeping only the resonant driving terms, equations (18) and (19) become

$$(-\omega_1^2 + \omega_p^2 + k_1^2c^2)\, A_{1y} = (\omega_p^2/2N_o)A_o n^* \qquad (23)$$

$$(-\omega_2^2 + c_s^2k_2^2)\, n = (Ze^2N_ok_2^2/mMc^2)A_oA_{1y}^* \qquad (24)$$

Taking the complex conjugate of equation (24) and eliminating n^* in equation (23) yields

$$(-\omega_1^2 + \omega_p^2 + k_1^2c^2)(-\omega_2^{*2} + c_s^2k_2^2) = (Ze^2\omega_p^2k_2^2/2mMc^2)A_oA_o^* \qquad (25)$$

Now using equation (21), letting $\omega_2 = \omega_{2r} + i\gamma_o$ where $\omega_{2r}^2 = c_s^2k_2^2$, $\gamma_o << \omega_{2r}$, and using $k_1^2 = k_o^2$, we have finally the homogeneous growth rate in the absence of damping[4]:

$$\gamma_o = -k_2v_o\omega_{pi}(8\omega_o\omega_2)^{-\frac{1}{2}} \qquad (26)$$

where $\omega_{pi}^2 = (Zm/M)\omega_p^2$, and $v_o = (e/mc)A_o$ is the electron 'jitter' velocity. For parameters typical of our experiments ($I = 10^{16}$ W/cm^2 or $v_o = 10^9$ cm/sec, $\lambda_o = 1$ μm), we see that $\gamma_o = 10^{13}$ sec^{-1}. The homogeneous growth rate is indeed large, even on picosecond time scales.

B. Quasi-Modes

Using equation (25), it is possible to examine the situation where the electromagnetic pump is so strong that it dominates the restoring force due to the electron

pressure, namely, $\omega_2 >> k_2 c_s$. These waves are called quasi-modes[5], since they do not obey the usual ion-acoustic dispersion relation. Using $\omega_2 >> k_2 c_s$ in equation (25), and solving for the growing root, we have

$$\omega_2 = \frac{1 - i\sqrt{3}}{2} \left\{ \frac{k_o^2 v_o^2}{\omega_o} \omega_{pi}^2 \right\}^{1/3} \tag{27}$$

with the requirement that

$$(v_o/v_e)^2 >> 4\omega_o c_s k_2/\omega_{pe}^2 \tag{28}$$

where again $k_2 = 2k_o$. We note that the frequency of the quasi-modes depends on the incident intensity to the one-third power.

C. Linear Theory For Inhomogeneous Plasmas

We now consider Brillouin scattering in an inhomogeneous plasma. The linearized problem has been extensively described in the literature[1,4,6], and only the main points will be reviewed here. It is customary to define the wavenumber mismatch K(x) as

$$K(x) = k_o(x) - k_1(x) - k_2(x) \tag{29}$$

where, as before, the subscripts 0, 1, 2, refer to the incident electromagnetic wave, the backscattered wave, and the ion-acoustic wave, respectively. Since the plasma parameters may vary with position, the wavenumbers depend on x, and, in general, it will be possible to

satisfy the matching conditions exactly (K = 0) only at one point in space. The growth of the waves will be limited to a region around that point such that the total phase mismatch is small; i.e.,

$$\left|\int K(x)\, dx\right| < (\pi/2) \quad .$$

For simplicity, one usually considers plasma parameters which are linear functions of position:

$$\omega_p^2(x) = \omega_p^2 \, (1 - x/L_n) \tag{30}$$

$$T_e(x) = T_e \, (1 - x/L_T) \tag{31}$$

$$u(x) = u_o \, (1 - x/L_u) \tag{32}$$

u is the plasma fluid velocity. In the presence of a non-zero fluid motion, the ion-acoustic wave will be Doppler shifted, and its dispersion relation is[1]

$$\omega = (\underline{k}\cdot\underline{u} + kc_s)(1 + k^2\lambda_D^2)^{-\frac{1}{2}} \tag{33}$$

The factor inside the square root comes from charge separation effects, which were neglected when we used quasi-neutrality in the first section. We will usually use the limit $k^2\lambda_D^2 << 1$.

Rosenbluth has shown[6] that, for a wavenumber mismatch approximated by

$$K(x) = K'(0)\, x \ , \tag{34}$$

the instability is convective, with a spatial amplification, in the absence of damping, given by

$$I = I_o \exp(2\pi\lambda_\beta) \tag{35}$$

where $\lambda_\beta = (\gamma_o^2/K'v_-c_s)$ (36)

γ_o is the homogeneous growth rate (equation (26)), and v_- is the group velocity of the backscattered wave; $v_- = c^2|k_1|/\omega_1$. I is the intensity of the backscattered wave, and I_o is its initial (thermal noise) intensity. Clearly, substantial amplification requires $\lambda_\beta > 1$. For the linearized plasma parameters given by equations (30), (31), and (32), K' is found to be[4]

$$K' = (\omega_o/c)\{(\omega_p^2/\omega_o^2)(1/L_n) - (2/L_u)\} +$$

$$-k_2\omega_{pi}(\omega_{pi}^2 - \omega_2^2)^{-\frac{1}{2}}[(1/2L_T) + (\omega_2^2/2L_n)(1/(\omega_{pi}^2 - \omega_2^2))] \qquad (37)$$

To find the instability threshold, we require the amplification factor λ_β to be order one. Specializing to $\omega_{pi} >> \omega_2$, and $k_2 = 2k_o$, the threshold is given by[4]

$$(v_o/v_e)^2 > 4\{(c/\omega_o L_n)[1 - (4v_e^2 ck_o^3\omega_o/\omega_{pe}^4)] +$$

$$-(c^2k_o/L_T\omega_{pe}^2) - (2c\omega_o^2/L_u\omega_o\omega_{pe}^2)\} \qquad (38)$$

In our experiment, the plasma is approximately isothermal throughout the region of interest, so $L_T \to \infty$. Also, for $k^2\lambda_D^2 << 1$, the second term may be neglected. The two remaining terms describe the effects of the wavenumber mismatch of the electromagnetic waves due to the changing density, and the changing ion-acoustic wavenumber due to the position dependent flow velocity. For most plasmas of interest for laser fusion, the fluid velocity increases

as one moves toward lower densities, so that L_u is negative in equations (32) and (38), and in (39) below. With the approximations mentioned above, the amplification factor, given by equation (36), is

$$\lambda_\beta = (1/8)(v_o/v_e)^2(\omega_p/\omega_o)^2 k_o\left[(1/2L_n)(\omega_p/\omega_o)^2-(1/L_u)\right]^{-1} \tag{39}$$

This is the spatial amplification of a backscattered wave in an inhomogeneous plasma. In equations (38) and (39), $u_o >> c_s$ has been assumed. For $u_o << c_s$, the following replacement is made:

$$(1/L_u) \rightarrow (M^*/L_u) \tag{40}$$

where M^* is the Mach number, (u_o/c_s). We see that subsonic flows reduce the importance of velocity gradients. Inserting parameter values of the order expected in these experiments ($(v_o/v_e) \sim 1$, $(\omega_p/\omega_o) = 0.5$, $L_n = -L_u = 20\ \lambda_o$), we see that $\lambda_\beta > 1$, so that large backscatter is predicted.

It should be noted that the theory thus far presented is a linearized one; that is, the incident wave is considered to be large and unchanging, while the backscattered and ion-acoustic waves are small and growing. Only resonant interactions between the incident wave and one of the small waves are considered. However, when the backscatter grows large, other terms may be important. For example, it has been shown[7] that

when the ion-acoustic wave grows large ($\{n/N_o\} > k^2\lambda_D^2$), strong harmonic generation occurs. These harmonics can interact with the pump wave to drive backscatter at $(\omega_o - 2\omega_2)$, $(\omega_o - 3\omega_2)$, etc., while the fundamental backscatter at $(\omega_o - \omega_2)$ continues to drive the acoustic wave. Another complication we have ignored is the possibility of two or more stimulated scatterings taking place in the plasma[8]. For this to occur, the back-scattered waves must be comparable to the pump wave, so the linear theory is no longer applicable. Additional problems include pump depletion, the strong Landau damping which occurs when the ion temperature approaches the electron temperature, and other non-linear dissipation mechanisms such as ion trapping and wave breaking. The proper treatment of these non-linear effects in limiting Brillouin scattering is currently as area of active research. Some of the ideas involved will be reviewed in the next section.

D. Non-Linear Models of Brillouin Scattering

Non-linear models of Brillouin scattering generally assume that the density perturbation has saturated at a value δn. Some of the possible saturation mechanisms are listed at the end of the previous section. We assume that the amplitudes of the backscattered and incident

waves are slowly varying functions of position; i.e.,

$$\underline{A}_1 = \underline{A}_1(x)\cos(\omega t - k_1 x) \tag{41}$$

where $k_1 A_1' >> A_1''$,

and similarly for the incident wave $\underline{A}_o$. Consider a plasma of constant density N_o and length L. Then substitution of (41) into the wave equation (9) yields[9,10]

$$\frac{d}{dx} A_1 = -\alpha \frac{\delta n}{N_o} A_o \tag{42}$$

and similarly for the incident wave

$$\frac{d}{dx} A_o = -\alpha \frac{\delta n}{N_o} A_1 \tag{43}$$

where

$$\alpha = (\omega_p^2/4k_1c^2) = (\pi/2)(N_o/n_c)(1/\lambda_o)\left[1-N_o/n_c\right]^{-\frac{1}{2}} \tag{44}$$

and where λ_o is the vacuum wavelength. As in the linear case, the non-resonant driving terms have been dropped. If we normalize the incident wave to one ($A_o(0) = 1$), and assume that the initial backscatter noise level is small ($A_1(L) = 0$), then the solution to equations (42) and (43) is

$$A_o = \left(e^{\theta x/L} + e^{2\theta} e^{-\theta x/L}\right)\left(1 + e^{2\theta}\right)^{-1} \tag{45}$$

$$A_1 = \left(-e^{\theta x/L} + e^{2\theta} e^{-\theta x/L}\right)\left(1 + e^{2\theta}\right)^{-1} \tag{46}$$

where $\theta = \alpha L(\delta n/N)$

The reflectivity is given by

$$r = |A_1(0)/A_o(0)|^2 = \tanh^2(\theta) \tag{47}$$

We will now consider two of the possible mechanisms which can limit the size of the ion wave, starting with ion trapping[7]. When the wave amplitude grows to a value such that the ion velocities are affected, then trapping can occur. Specifically, the ions which have velocities comparable to the wave's phase velocity feel the potential of the wave for a long period of time. The ions are accelerated; the energy they gain is lost from the wave. This loss limits the wave amplitude. A crude estimate of the value of $\delta n/N$ for which trapping occurs may be obtained by modeling the distribution with the water-bag model[11]. (In this model, the ion distribution function is a constant for $|v| < \sqrt{3}\, v_i$, and zero otherwise.) Calculating the size of the wave where the ion velocity (driven plus thermal) equals the wave velocity, one finds

$$(\delta n/N) = (1/2)\left\{(1 + (T_i/T_e))^{\frac{1}{2}} - (3T_i/T_e)^{\frac{1}{2}}\right\}^2 \qquad (48)$$

Since we will see that this model has serious failings if the ion temperature is comparable to the electron temperature, we will take, as an example, $(T_i/T_e) = 0.1$. Then equation (48) gives $(\delta n/N) = 0.13$. Continuing the example, if $N = 0.2\, n_c$, and $L = 20\, \lambda_o$, then equation (47) predicts a reflectivity of 50%. Clearly, ion trapping does not limit the Brillouin scattering to small values.

We now consider the possibility of the size of the ion wave being limited by harmonic generation. For finite $\delta n/N$, the plasma's phase space characteristics intersect[7], indicating that shock waves can form there. Near the intersection, the waveform steepens, generating harmonics. The time for a disturbance to propagate to the shock point is

$$t_1 = \pi\left(2\,\omega\,(\delta n/N)\right)^{-1} \tag{49}$$

However, no shock will form if the plasma is too dispersive; that is, if the harmonics are appreciably out of phase (say, by $\lambda/4$) with the fundamental at t_1. To estimate the dispersion time, the complete dispersion relation must be used:

$$\omega^2 = c_s^2 k^2 \left(1 + k^2 \lambda_D^2\right)^{-1} \tag{50}$$

We then find the time for the fundamental and second harmonic to be out of phase:

$$t_2 = \pi\left(3\omega k^2 \lambda_D^2\right)^{-1} \tag{51}$$

Equating t_1 and t_2, we find the condition for harmonic generation:

$$(\delta n/N) = k^2 \lambda_D^2 \tag{52}$$

If this limit is exceeded, the wave's energy cascades into the harmonics. Applying the same parameters we used previously ($N = 0.2\ n_c$, $L = 20\ \lambda_o$) and taking $T_e = 2$ KeV,

equation (52) gives $(\delta n/N) = 0.06$, and equation (47) predicts a reflectivity of 17%, considerably lower than the ion-trapping limit. It should be noted that equation (47) predicts a drastic increase in Brillouin scattering for increasing scale lengths. For example, if we use $L = 40\ \lambda_0$ in the above example, the reflectivity increases to 50%.

We now review a model, due to Kruer[12,13], which takes into account the finite amount of ion heating. It is well known[14] that ion-acoustic waves are strongly (ion) Landau damped, unless $(ZT_e/T_i) >> 3$. Ion-trapping by the wave produces a 'tail' of energetic ions; however, the model assumes, for simplicity, that the effect is similar to uniform heating of the ions[15]. Since the ions are warm, they Landau damp the acoustic wave. This damping, in turn, deposits more energy into the ions; the ion temperature rises, and this increases the damping. Thus, we have a negative feedback mechanism which seeks to limit the size of the ion-acoustic wave.

To calculate the size of the wave, we must use equation (13). As before, only the resonant terms are kept, yielding

$$\frac{\delta n}{N_o} = \frac{Ze^2k^2}{2m_i M\omega\nu c^2}\ A_o A_1 \qquad (53)$$

where ω is the ion-acoustic frequency, and ν is the Landau damping rate, given by[14]

$$\nu = \omega\sqrt{\pi/8}\ (ZT_e/T_i)^{3/2}\exp(-ZT_e/2T_i) \qquad (54)$$

where $k^2\lambda_D^2 << 1$ has been assumed. It should be noted that, for our experiments using silicon dioxide plasmas, the proper Z to use in equation (54) is the charge state of the oxygen ions. Not only are they the most abundant species, but they are also the lightest; their thermal velocity is larger, and they therefore damp the acoustic wave more effectively. (The exponent in equation (54) should have $M_j\langle Z/M\rangle$ instead of simply Z, where M_j is the mass of the j^{th} species, and $\langle\ \rangle$ denotes a species average. For our plasmas, however, $\langle Z/M\rangle = Z_j/M_j$ for all species. Thus the exponent is smallest for the smallest mass, and $M_j\langle Z/M\rangle = Z_j$.)

Equations (42), (43), and (53) can be solved for the reflectivity[13,16], for a plasma of density n and length L:

$$r(1 - r) = B(\exp[q(1 - r)] - r) \qquad (55)$$

where

$$q = (k_oL/4)(n/n_c)(\omega/\nu)(v_o/v_e)^2(1-n/n_c)^{-1}(1+3T_i/ZT_e)^{-1} \qquad (56)$$

Here B is the initial noise level of the backscattered wave ($B = A_1(L)$), k_o is the vacuum wavenumber of the incident wave, $v_o = (eA_o/mc)$, and $v_e^2 = T_e/m$. The damping rate, ν, depends on the ion temperature (see equation (54)).

To estimate T_i, it is assumed that all of the acoustic wave energy is going into heating the ions, and that the ions are transporting the energy away as fast as possible (free streaming). Equating these two terms gives

$$rI_o\omega/\omega_o = n_i v_i T_i \tag{57}$$

Here rI_o is the fraction of the incident wave undergoing Brillouin scattering, and $(\omega/\omega_o) = 2k_o c_s/\omega_o$ is the fraction of the scattered energy which goes into the ion-acoustic wave. Equations (55) and (57) can be solved iteratively for the reflectivity, r. For example[13], if $n = 0.2n_c$, $T_e = 6$ KeV, and $I_o = 3\times10^{15}$ W/cm^2 at $\lambda_o = 1$ μm, then r = 10% for $L = 10\lambda_o$, and r = 40% for $L = 100\lambda_o$. As predicted earlier, we see that ion heating has a negative feedback effect; the increase in back-scatter with increasing scale length is much slower than was predicted when ion heating was ignored (equation (47)).

Finally, an estimate can be made for the time required to heat the ions to $T_i = ZT_e/3$. Assuming r is a constant, one gets[13]

$$t_h = L(n/n_c)(v_e/v_o)^2(1/3c_s r) \tag{58}$$

as the time required to heat the ions. For the example above, with $L = 100\lambda_o$, $t_h = 100$ psec. It should be noted that equation (58) overestimates the time required for ion damping to be important. Inspection of the damping rate, equation (54), shows that the damping is a maximum

for $ZT_e/T_i = 3$; however, it is still appreciable for much larger temperature ratios. For example, if $ZT_e/T_i = 12$, then equation (54) gives, for $\lambda_o = 1\ \mu m$ and $T_e = 1$ KeV, $\nu^{-1} = 6$ psec.

E. Hydrodynamics

We will now review two of the aspects of the coronal hydrodynamics which can effect our experiment. First of all, as was pointed out in equation (39), velocity gradients can limit the size of the phase-matching region, by Doppler shifting the acoustic wave frequency. These gradients are likely to be large in plane target experiments, due to the one dimensional nature of the expansion. They may also be large in short pulse experiments, where hydrodynamic steady state may not be reached during the laser pulse. However, in our prepulse experiments, the plasma has time to expand into a quasi-steady state flow. Our measurements will show that the density profile is well described by an exponential over the range of 1 to 9×10^{20} cm^{-3}. If we assume that it is exponential everywhere ($n = n_c \exp(-z/L_n)$), and that we have steady state flow, then we can use the continuity equation ($\nabla\cdot(n\underline{v}) = 0$) to find the velocity as a function of z, the distance from the critical surface. Defining the velocity scale length in the usual fashion,

$$L_u = v(dv/dz)^{-1}$$

we find

$$L_u = L_n(R + z)/(R + z - 2L_n) \qquad (59)$$

where R is the radius to the critical density, and z is the radial distance measured from the critical surface. For our parameters of R = 40 μm, and L_n from 10 to 40 μm, equation (59) shows that the velocity scale lengths are always greater than the density scale lengths. Furthermore, L_u is particularly large in the density region of 0.1 to 0.5 of critical density, especially for density scale lengths of 20 μm or more. Therefore, the velocity gradients are not of great importance in limiting the phase-matching length at densities near critical density.

The plasma hydrodynamics can effect the interpretation of the spectral data. If the critical surface is moving, or if ions are flowing through the critical surface, the reflected light will be Doppler shifted[17]. Since this shift is toward shorter wavelengths for plasma motion outward, it can mask or confuse the interpretation of the Brillouin shift toward longer wavelengths. When there is no prepulse, this is indeed the case. With a prepulse formed plasma, however, the hydrodynamic motions have time to relax to a quasi-steady state. Further evidence in support of this statement is the observation[18] that, with long pulse irradiation, the critical surface

moves out rapidly for the first ~70 psec, but then assumes a more or less stationary position for the duration of the pulse. Since the Doppler shift is $\Delta\lambda/\lambda = 2v/c$, critical surface velocities of less than 6×10^6 cm/sec will produce spectral shifts of less than 4 Å.

One can also use a steady state, isothermal model[18] to estimate the plasma flow velocity. For short pulse experiments, the isothermal assumption is not particularly accurate, so the results should be considered as order of magnitude estimates. The equation of motion may be integrated to obtain

$$v^2 = 2c_s^2 \ln(n_s/n) + v_s^2 \qquad (60)$$

where c_s is the ion-acoustic speed, n_s and v_s are the density and velocity at the plasma source. One usually assumes $(n_s/n) >> 1$, and $c_s >> v_s$. Similarly, the mass conservation equation (steady state) may be integrated, giving

$$r^2 nv = (1/4\pi)(\dot{m}/M_i) \qquad (61)$$

where $\dot{m}$ is the (constant) rate of mass flow, in a spherically symetric geometry. Equation (60) predicts an outward flow velocity of approximately $2c_s$ in the vicinity of the critical surface. This flow of material into the underdense region can give rise to a spectral shift toward shorter wavelengths. For a one dimensional

expansion, the shift is given by[17]

$$(\Delta\lambda/\lambda) = -(u/c) \tag{62}$$

where u is the flow velocity at the critical surface. However, for a three dimensional steady state flow, the magnitude of this shift is reduced by the factor $(R_c/R_F)^2$ where R_c is the radius of the critical density, and R_F is the radius of the expansion front. This extra factor, which is due to the three dimensional steady state continuity equation ($\nabla\cdot(r^2 n\underline{v}) = 0$), can reduce the predicted blue shift by an order of magnitude or more. This is especially true for prepulse formed plasmas, where $R_F >> R_c$.

III. EXPERIMENTAL PROCEDURES

A. Introduction

There are two specific objectives in this thesis. The first is to present data showing the relationship between the density gradient and the amount of stimulated backscatter produced, when a spherical glass microshell is illuminated with a high power laser. In the following sections, we describe the laser system, and the diagnostics used for these measurements; the optical probe beam and holographic interferometry, and the calorimetry. The numerical procedures used to unfold the interferometric data are discussed in chapter IV.

The second objective of this work is to examine the spectral content of the backscattered energy, with emphasis on time resolved spectroscopy. The procedures and equipment used for these measurements are described in the final two sections of this chapter.

B. Glass Development Laser

The Laboratory For Laser Energetics' Glass Development Laser[1] (GDL) is a one beam, phosphate glass system capable of peak powers in excess of 0.5 TW in short pulses. Figure 2 shows a schematic diagram of the laser

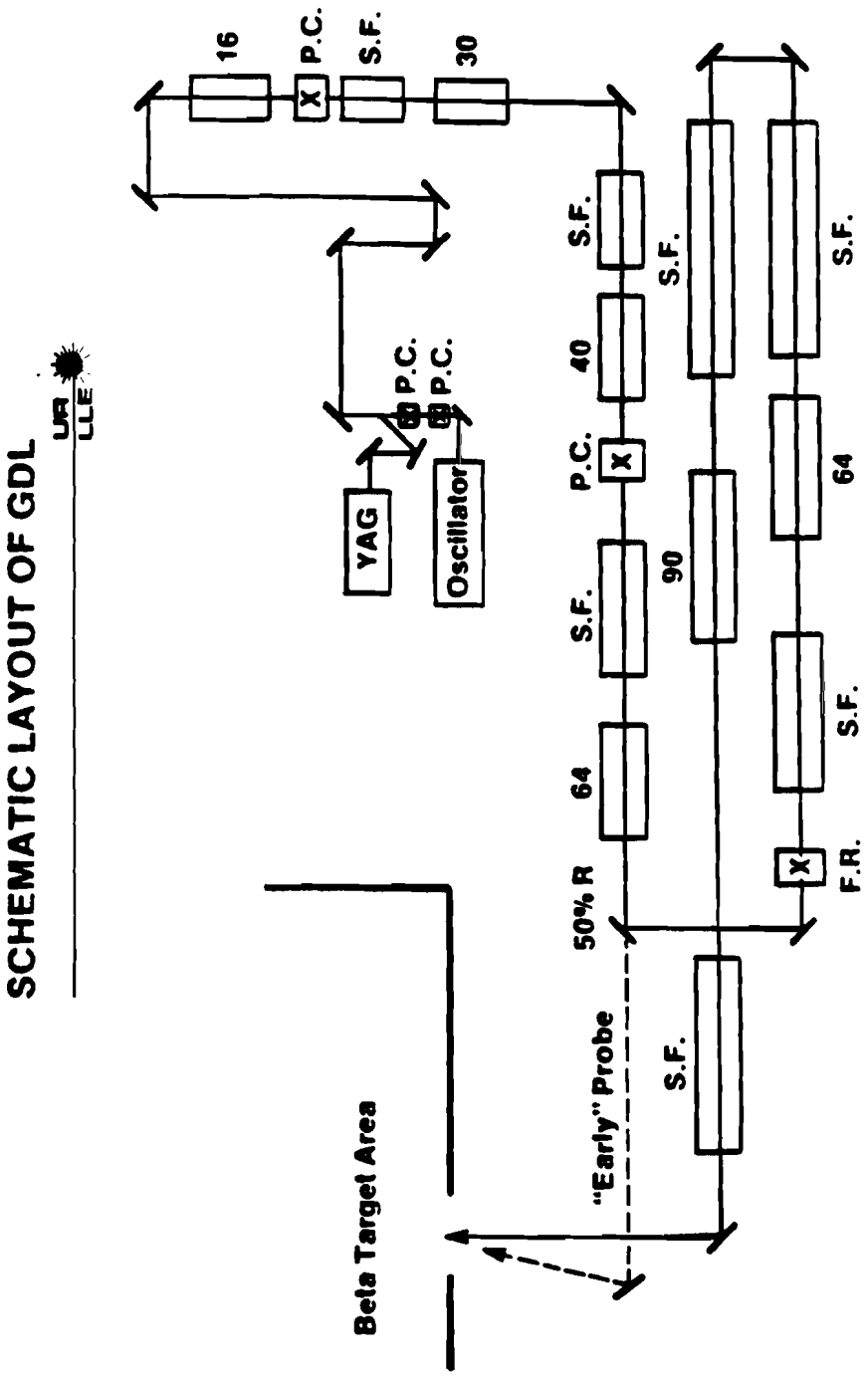
SCHEMATIC LAYOUT OF GDL
UR
LLE
16
P.C.
S.F.
30
YAG
Oscillator
P.C.
P.C.
S.F.
40
P.C.
S.F.
90
64
50% R
"Early" Probe
S.F.
S.F.
S.F.
64
S.F.
F.R.
Beta Target Area

Figure 2

system. Notice that there are two beams exiting the room; one is the output of the last laser amplifier, while the other contains half of the energy output of the first 64 mm rod amplifier. This latter beam will be referred to as the 'early' probe beam.

The GDL system was slightly modified to allow for the introduction of a controlled prepulse. The prepulse insertion system is shown in Figure 3. A translation stage, holding the retroreflecting prism, makes it possible to adjust the prepulse timing from 0.5 nsec, to 1.8 nsec, before the main pulse. The two half-wave plates, in conjunction with the polarizer P, independently adjust the intensity of the main pulse and the prepulse. The main pulse is always reduced by at least a factor of two, to avoid overdriving the laser system. Therefore, ratios of prepulse energy to main pulse energy of zero to ten percent are available.

The prepulse system was assembled as follows. First, the retroreflecting prism was adjusted, with a helium-neon laser, to have its front face orthogonal to the direction of motion of the sliding stage. This assembly was then inserted into the prepulse system, and mirror M2 adjusted to bring the YAG alignment beam orthogonal to the prism's front surface. This left the laser beam parallel to the slide direction, so that when

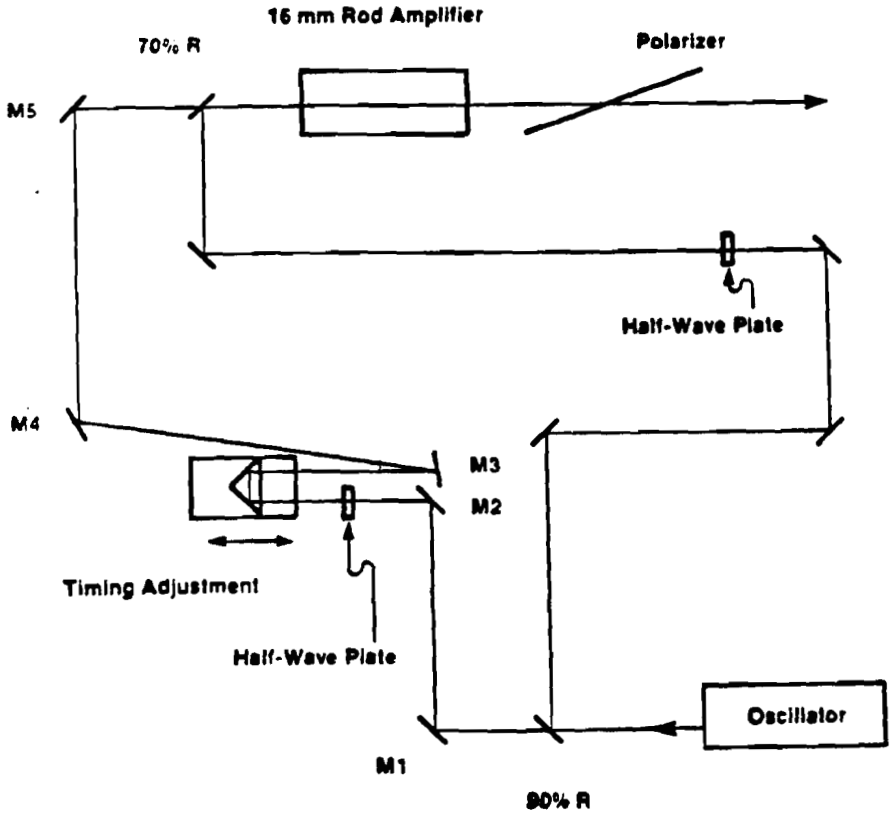

Figure 3. Prepulse System

the stage was translated back and forth, there was no change in the location of the retroreflected beam on M3. Mirrors M4 and M5 were then used to insert the prepulse back into the laser system.

Measurement of the relative timing between the prepulse and the main pulse was accomplished using a vacuum photodiode and a Tektronics 7844 oscilloscope. The half-wave plates were adjusted so that the prepulse and main beam were of approximately equal intensity, and a low power shot, firing only the first 4 rod amplifiers, was taken. From the resulting oscilloscope trace, the prepulse to main beam time difference was found to be 1.8 nsec. The accuracy, limited mainly by the rise time of the scope and 80 feet of RG-59 cable, is estimated at 0.2 nsec. The position of the translation stage was noted, and all subsequent prepulse times were calculated from $t = 1.8(\text{nsec}) - 2d/c$, where $2d$ is the distance by which the path length was increased. Since this can easily be measured to millimeter accuracy, the reproducibility of any setting is accurate to within a few picoseconds.

We will end this section with a brief description of the target area, also known as Beta. A schematic diagram is shown in Figure 4. At the first mirror the GDL beam encounters in the target room, four percent of

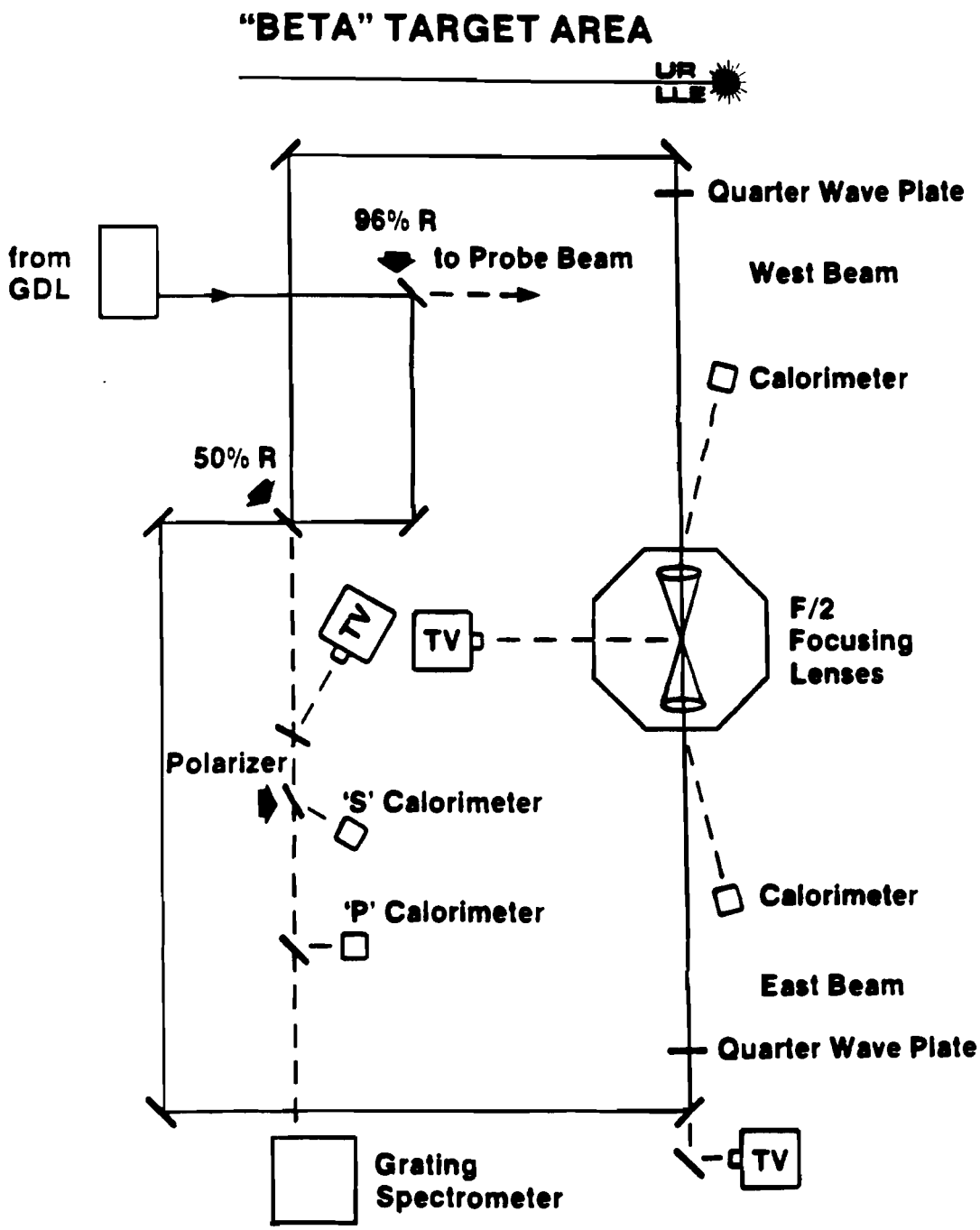
"BETA" TARGET AREA
UR
LLE
Quarter Wave Plate
96% R
from
GDL
to Probe Beam
West Beam
Calorimeter
50% R
TV
TV
F/2
Focusing
Lenses
Polarizer
'S' Calorimeter
'P' Calorimeter
Calorimeter
East Beam
Quarter Wave Plate
TV
Grating
Spectrometer

Figure 4

the energy is transmitted and directed to the probe beam table. This beam will be referred to as the 'synchronous' or 'main' probe beam, to distinguish it from the early probe beam. The remaining ninety six percent of the energy is then split into two approximately equal intensity beams, which are directed through quarter-wave plates and into the vacuum chamber from opposite directions. Inside the chamber, F/2 aspheric lenses focus the beams onto the target. The quarter-wave plates are oriented to give right circular polarization.

A videcon is positioned to view the target through the fifty percent beamsplitter; it observes the back-reflected light of the YAG alignment laser, insuring proper focus. (A 50 μm correction is applied to the focusing lenses to compensate for the chromatic shift due to the 100 Å difference between YAG and phosphate glass lasing wavelengths.) This backscatter viewing system was also used to confirm the proper alignment of the prepulse insertion system, by allowing the YAG to propagate only along the path taken by the prepulse, and checking that it too was properly focused on target.

C. Ultraviolet Probe Beam

A synchronous, ultraviolet probe beam was constructed, so that the electron density could be measured